Lithium Niobate Film Bulk Longitudinal Wave Resonator

A. Reinhardt, M. Bousquet, A. Joulie, C.-L. Hsu, F. Delaguillaumie,
C. Maeder-Pachurka, G. Enyedi, P. Perreau, G. Castellan, J. Lugo
Univ. Grenoble Alpes
CEA-LETI
MINATEC Campus, Grenoble, France
alexandre.reinhardt@cea.fr

***Abstract*—Film bulk acoustic wave resonators (FBAR) based on $LiNbO_3$ single crystal piezoelectric films offer promising perspectives towards wide bandwidth filters. We present resonators based on the Y+36° crystal orientation, which promotes the excitation of longitudinal waves. This allows reaching resonance frequencies of 4.3 GHz for 600 nm-thick films, with electromechanical coupling factors of 21.4%, quality factors of 255 and impedance ratios of 245 and a temperature coefficient of frequency of -60 ppm/K, which is lower than previously reported with shear wave resonators. The resonators have also proved to withstand operation under at least 25 dBm continuous power, being limited only by the measurement setup.**

Keywords—FBAR, $LiNbO_3$, longitudinal waves, sub-6 GHz filters.

I. INTRODUCTION

The fourth and fifth generations of mobile communication systems (4G, 5G) have opened frequency bands in the 3 to 5 GHz range. Among these bands, n77, n78 and n79 exhibit fractional bandwidths between 12 and 24 %. A filter covering these bands would ideally require resonators with electromechanical coupling factors ranging from 20 to 50 %. This has motivated in the last years the development of resonators based on single crystal $LiNbO_3$ and $LiTaO_3$ thin films. The most mature application is certainly the Incredibly High Performance Surface Acoustic Wave (IHP-SAW) and its equivalents [1-4]. To increase the operation frequency while maintaining reasonable interdigitated electrodes dimensions, the search for waves with increased phase velocities has led to the development of longitudinal leaky SAW propagating in a piezoelectric thin film and prevented from radiating in the substrate by using multilayer reflectors [5]. In parallel, resonators and filters exploiting the first antisymmetric Lamb mode propagating in lithium niobate membranes show great promises [6-8].

Comparatively, bulk acoustic wave (BAW) resonators have received less attention despite early demonstrations tracing back 2007 [9] and the potential to provide large electromechanical coupling factors [10]. We have recently investigated the scaling of shear wave Film Bulk Acoustic Resonators (FBAR) towards the sub-6 GHz range [11]. With wave velocities close to 4540 m/s, Y+163° resonators require piezoelectric films with a thickness of 250 nm to reach 4.8 GHz. For such low thicknesses of piezoelectric films, we could conclude that the electrodes make a significant part of the resonator stack, hence providing adverse effects in terms of mechanical damping and contribution to the temperature coefficient of frequency. Additionally, at such low thicknesses, residual defects from the crystal ion slicing process used to transfer the single crystal piezoelectric film can rapidly degrade resonator performances [11].

To overcome these limitations, it is therefore necessary to rely on piezoelectric films as thick as possible. Operation in the sub-6 GHz range requires therefore relying on longitudinal waves, which exhibit significantly faster wave velocities than shear waves.

II. METHODS/RESULTS

The most common way to obtain lithium niobate thin films is through layer transfer techniques [10]. In this case, the choice of original $LiNbO_3$ substrate orientation defines directly the crystal orientation of the piezoelectric thin film. Fig. 1 shows the dependency of the electromechanical coupling factor of longitudinal waves propagating in lithium niobate films as a function of the original wafer cut angle. The material constants for $LiNbO_3$ determined by Kovacs *et al.* [12] where used in this calculation. The maximum electromechanical coupling factor is 25.3% for a cut angle of 31°. Fig. 1 shows however than for

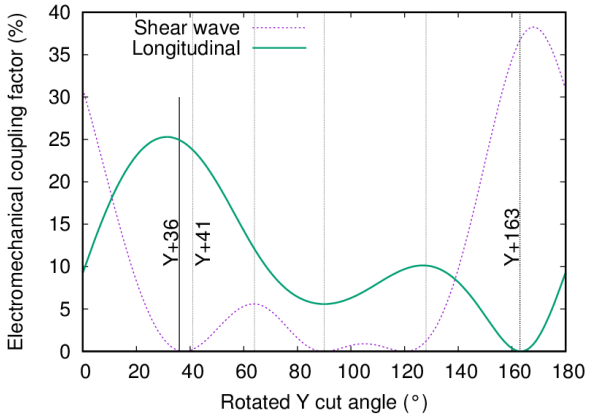

Fig. 1. Electromechanical coupling factor of bulk waves propagating in lithium niobate films as a function of the cut-angle of the original wafer. Vertical lines represent common commercial cuts.

This work was supported by the French National Research Agency funding ANR LiLit (ANR-16-CE24-0022-011).

978-1-6654-3935-0/21/$31.00 ©2021 IEEE

this cut, one of the shear waves still exhibits a coupling factor of close to 1%. Single mode operation is reached for the Y+38° orientation. For the sake of simplicity, we opted for the Y+36°, for which commercial wafers are commonly available. In this case, the electromechanical coupling factors for the longitudinal and shear waves are respectively 24.9% and 0.07%. In addition, the large difference in wave velocities (7320 m/s for the longitudinal wave vs. 4020 m/s for the weakly coupled shear wave) ensures single mode operation in practice.

We fabricated a set of FBAR using a previously reported process flow [10, 11]: here a Y+36° $LiNbO_3$ wafer is ion-implanted to induce sub-surface crystalline defects. On one of the samples, a Pt bottom electrode is evaporated and then patterned by ion beam etching. On the other samples, AlSi bottom electrodes are sputtered and patterned by wet etching. An amorphous silicon sacrificial layer is then deposited by sputtering and patterned by dry etching. SiO_2 is deposited by reactive sputtering of a Si target and polished to leave a flat surface compatible with direct bonding onto a host wafer, here another Y+36° $LiNbO_3$ wafer coated with another SiO_2 layer. After bonding, a thermal treatment causes the implantation defects to grow until they cleave the initial donor wafer, leaving only a thin single crystal film attached to the host wafer. This film is then polished to smooth its top surface and to adjust its thickness to the target values (640 and 310 nm). Electrical contacts to the bottom electrodes and release holes giving access to the sacrificial layer are then etched by ion beam etching. An AlSi top electrode is sputtered and patterned by wet etching. Eventually, membranes are released by etching the amorphous silicon sacrificial layer with gaseous XeF_2.

After fabrication, we measured these devices using coplanar GSG probes connected to a Vector Network Analyzer. The setup was calibrated using a Short – Open – Load procedure, as the resonators were in single port configuration. The measurement power was set to -10 dBm. Raw responses, without any deembedding, are shown in Fig. 2. Three types of resonators were considered, with respective layer stacks: Pt 100 nm / $LiNbO_3$ 630 nm / AlSi 100 nm, AlSi 100 nm / $LiNbO_3$ 640 nm / AlSi 100 nm and AlSi 100 nm / $LiNbO_3$ 310 nm / AlSi 100 nm. As expected, the density of the bottom electrode and the thickness of the piezoelectric film influence the resonance frequency.

Interestingly, a resonator with a 640 nm $LiNbO_3$ film and 100 nm AlSi electrodes exhibits resonance and antiresonance frequencies of 4.35 and 4.81 GHz, resulting in an effective electromechanical coupling factor of 21.4%. As shown in Fig. 2, its electric response agrees very well with a Mason's model provided minute adjustment of the layer thicknesses to match precisely the measured frequencies. Its quality factor at antiresonance is evaluated as 255 and its impedance ratio to 245.

The resonator with Pt bottom electrodes provides an easier comparison with previously reported resonators operating in the 2 GHz range, even if its resonance and antiresonance frequencies are respectively 2.97 and 3.22 GHz, leading to an electromechanical coupling factor of 17%. The quality factor at resonance is 240 and the impedance ratio 214.

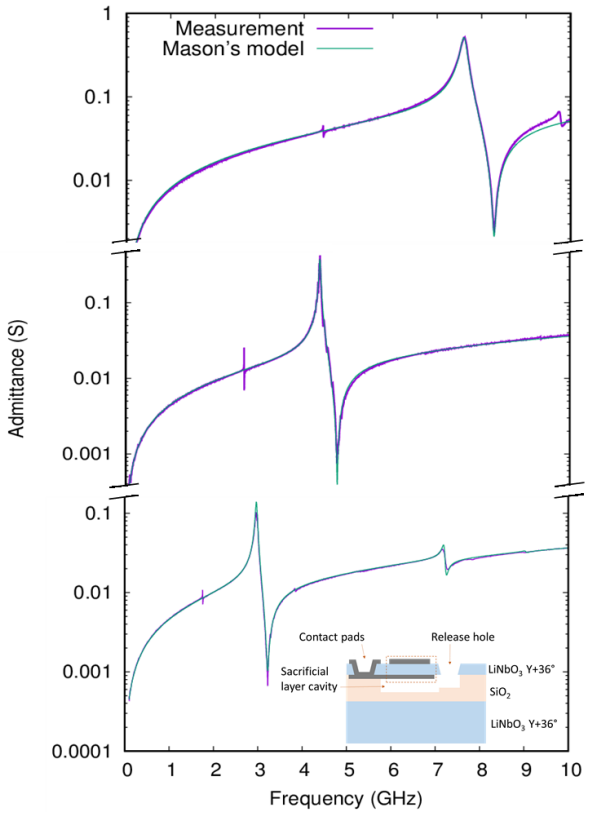

Fig. 2. Electric response of a Y+36° $LiNbO_3$ FBARs whose material stacks are respectively, from bottom to top: Pt / $LiNbO_3$ (630 nm) / AlSi, AlSi / $LiNbO_3$ (600 nm) / AlSi and AlSi / $LiNbO_3$ (300 nm) / AlSi. Fits using Mason's model are superimposed over each response. Inset is a schematic cross section of the resonator.

Decreasing the piezoelectric film to 300 nm pushes resonance and antiresonance frequencies to respectively 7.61 and 8.28 GHz, leading to an effective electromechanical coupling factor of 18.5%. The quality factor at antiresonance is then 160 and the impedance ratio 212.

These resonators were also measured versus temperature using the same experimental setup while heating the measurement chuck up to 150°C. The three different resonators types exhibited a linear behavior versus frequency, with temperature coefficients of respectively -73±5, -60±5 and -60±5 ppm/K for the resonance and -59±6, -54±5 and -66±5 ppm/K for the antiresonance. The comparison of the temperature dependences of the AlSi 100 nm / $LiNbO_3$ 600 nm / AlSi 100 nm and AlSi 100 nm / $LiNbO_3$ 300 nm / AlSi 100 nm resonators, which differ only by their piezoelectric films thicknesses, allows fitting independently the contributions of the electrodes and of the piezoelectric film to the temperature sensitivity. This provided a temperature coefficient of the acoustic velocities for longitudinal waves in Y+36° $LiNbO_3$ of -40 ppm/K. This is close to the theoretical value of -48 ppm/K obtained solving Christoffel's equation with the inclusion of the temperature dependence of the elastic constant and the influence of the thermal expansion on density.

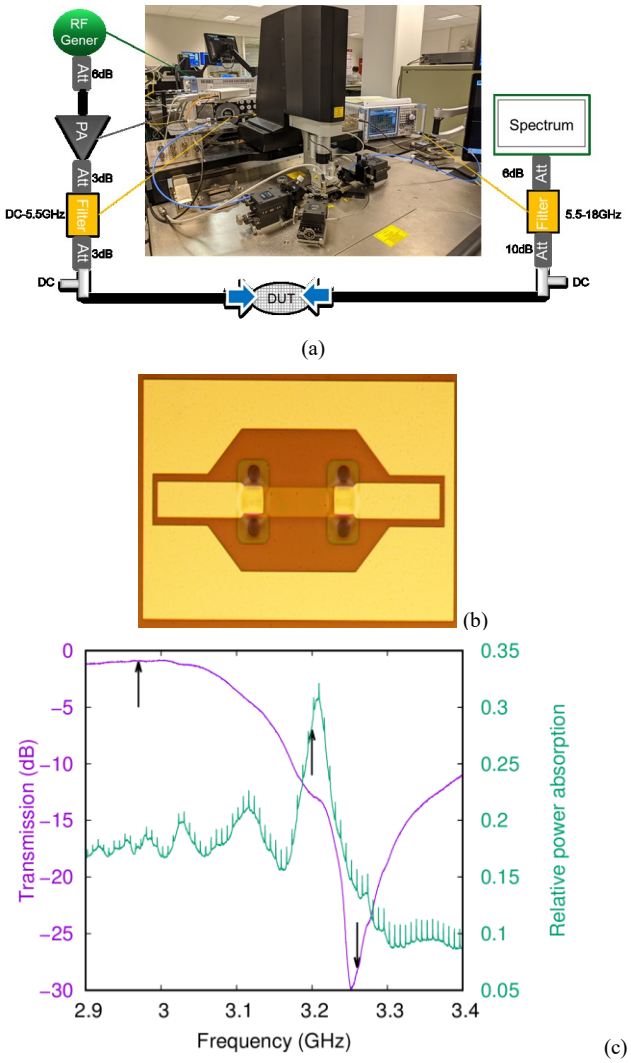

Fig. 3. Measurement setup for preliminary power handling and linearity measurements (a), optical micrograph of a set of resonators in series which were measured (b) and (c) identification of the frequency points of interest.

The fit also provided a temperature coefficient for the longitudinal acoustic velocity in our AlSi films of -170 ppm/K.

Finally, we initiated high power measurements of these resonators. The setup we used is shown Fig. 3(a): a single tone RF generator signal is amplified by a power amplifier. This signal is filtered to remove unwanted harmonics generated by the amplifier and applied at the input of a set of two resonators connected in series along the signal path, which are shown in Fig. 3(b). The output signal is then monitored by a spectrum analyzer, which extracts the spectral power density at the level of the fundamental frequency, and of the second and third harmonic. For initial explorations, we investigated the application of power close to the resonance and antiresonance frequencies, as well as at a frequency close to the point of maximum power absorption by the resonators, marked by arrows in Fig. 3(c). Due to limitations in the available components, we could only apply power up to 25 dBm. At this power level, we did not notice any degradation or irreversible change in the measured devices.

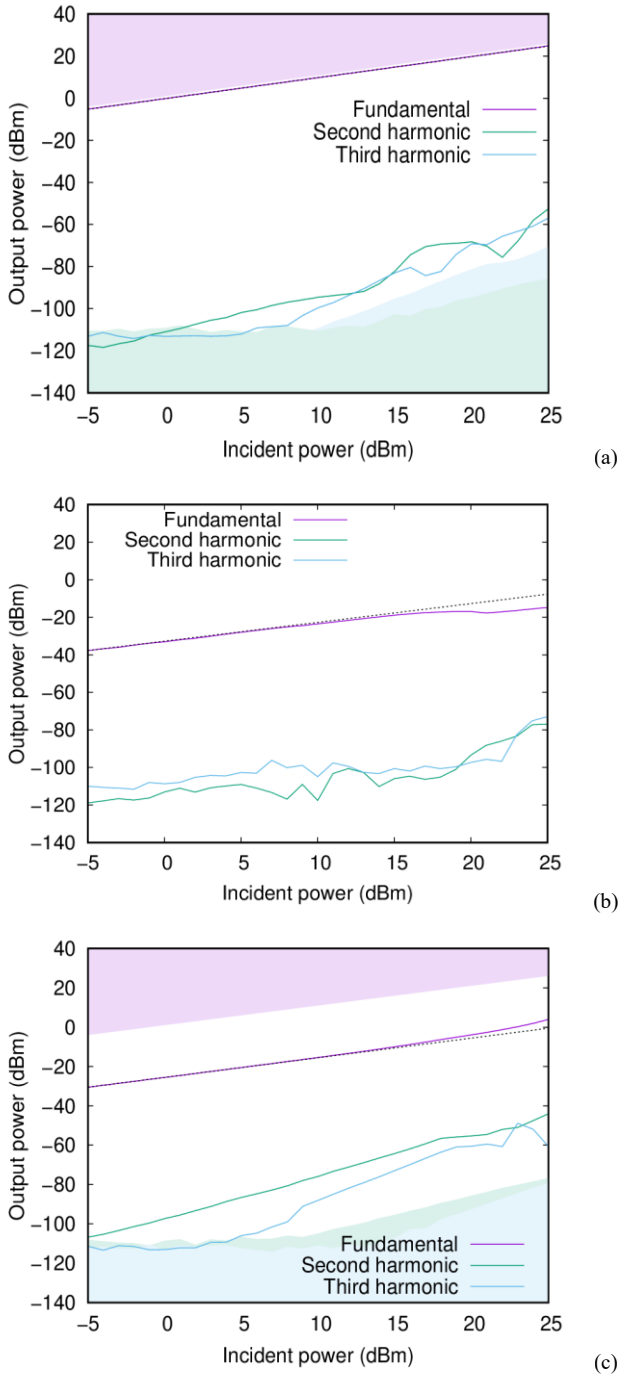

Fig. 4. Evolution of the fundamental, second and third harmonic spectral power density as a function of the incident power applied at the resonance frequency (a), the frequency of maximum power absorption (b) and the antiresonance (c). Shaded areas represent respectively the limits of perfect transmission (pink), and noise floors for the harmonic signals (blue and green).

Fig. 4 shows the evolution of the three main components of the output signal as a function of the applied power. As expected, the behavior depends on the frequency at which the signal is applied: at resonance, the output power at the fundamental frequency remains proportional to the input power, indicating nearly constant insertion loss. On the

contrary, when power is applied at the point of maximum power absorption or close to the antiresonance, variations in insertion loss appear. The increase of insertion losses in the first case and decrease in the second seems to indicate a possible decrease in frequency of the device, likely caused by self-heating under high power. A tentative to translate the evolution of the insertion losses into frequency shifts and then into temperature increases, based on the TCF evaluated previously, seems to indicate that the resonators reached temperatures up to 180°C when power is applied at the point of maximum power absorption and 120°C when power is applied at the resonance or the antiresonance. Obviously, these preliminary evaluations do not include other source of changes in insertion loss, such as increase in resistive losses with temperature, and thus the temperatures estimated by this method need to be confirmed by more direct temperature measurements.

Regarding the evolution of the second and third harmonic levels with incident power, extrapolations of their growths provide estimations of second and third order intercept points ranging from 65 to 90 dBm for IIP2 and 75 to 90 dBm for IIP3, depending on the frequency of the input signal and the geometry of the resonators which were measured. Here, the evolution of the insertion losses that is likely to be caused by self-heating induce also some uncertainties. Therefore, some further measurements at higher input power will be necessary to refine these estimations.

III. DISCUSSION/INTERPRETATION

The performances of the longitudinal wave resonators reported in this work compare favorably with previously reported shear wave resonators. The frequencies of operation are clearly higher than what we reported previously for Y+163° $LiNbO_3$ resonators based on similar stacks: 2.4 GHz for Al/X-cut $LiNbO_3$/Al resonators in [10] and 1.94 GHz for W / Y+163° $LiNbO_3$ / Al resonators in [13]. As indicated in Figure 1, this comes however at the cost of reduced electromechanical coupling factors. Interestingly, the larger wave velocities of longitudinal waves compared to shear waves make the resonators electromechanical coupling factors more robust to increases in operation frequencies, leading to relatively constant k^2 as the frequencies are increased up to 8 GHz in Figure 2. This is in striking contrast with Y+163° $LiNbO_3$ resonators whose electromechanical coupling factors proved more difficult to maintain at frequencies above 4 GHz in [11].

Another noticeable benefit from the Y+36° orientation is the lower temperature dependence for resonators operating at close to 5 GHz (TCF_r = -60 ppm/K) than what was reported for Y+163° resonators operating at the same frequency (TCFr = -190 ppm/K) [11]. The evaluation of the respective contributions of the AlSi electrodes and the piezoelectric film to the measured TCF indicate that the temperature sensitivity of the longitudinal wave resonators can be further decreased by changing the electrodes material.

IV. CONCLUSIONS

We have demonstrated the interest of film bulk acoustic resonators based on lithium niobate films promoting the excitation of longitudinal waves. The reliance on modes with large wave velocities allows reaching operation in the sub-6 GHz space with piezoelectric films close to 500 nm-thick. The lower electromechanical coupling factors of the longitudinal waves compared to shear waves is compensated by a lower temperature sensitivity compared to previously reported shear wave resonators and a better frequency-scaling of the quality factors. Finally, we have initiated some preliminary measurements at high power: resonators withstand at least -25 dBm incident power, limited only by the experimental setup used for the measurements. First estimations position IIP2 and IIP3 above 65 and 75 dBm, although additional measurements at higher input power will be needed to refine these estimations.

ACKNOWLEDGMENT

This work has been performed with the help of the “Plateforme Technologique Amont” de Grenoble, with the financial support of the “Nanosciences aux limites de la Nanoélectronique” Fundation and CNRS Renatech network.

REFERENCES

[1] T. Takai *et al.*, "Incredible high performance SAW resonator on novel multi-layerd substrate," 2016 IEEE International Ultrasonics Symposium (IUS), pp. 1-4, 2016.

[2] M. Kadota, Y. Ishii, T. Shimatsu, M. Uomoto and S. Tanaka, "Suprious-Free, Near-Zero-TCF Hetero Acoustic Layer (HAL)SAW Resonators Using $LiTaO_3$ Thin Plate on Quartz," 2018 IEEE International Ultrasonics Symposium (IUS), pp. 1-9, 2018.

[3] S. Inoue and M. Solal, "Layered SAW Resonators with Near-Zero TCF at Both Resonance and Anti-resonance," 2019 IEEE International Ultrasonics Symposium (IUS), pp. 2079-2082, 2019.

[4] S. Ballandras *et al.*, "Development of Temperature-Stable RF Filters on Composite Substrates Based on a Single Crystal $LiTaO_3$ Layer on Silicon," 2019 Joint Conference of the IEEE International Frequency Control Symposium and European Frequency and Time Forum (EFTF/IFCS), pp. 1-4, 2019.

[5] T. Kimura *et al.,* "3.5 GHz longitudinal leaky surface acoustic wave resonator using a multilayered waveguide structure for high acoustic energy confinement", Jpn. J. Appl. Phys. 57 07LD15, 2018.

[6] M. Kadota *et al.*, "High-frequency Lamb wave device composed of $LiNbO_3$ thin film", Jpn. J. Appl. Phys. 48 07GG08, 2009.

[7] V. Plessky *et al.*, "Laterally excited bulk wave resonators (XBARs) based on thin Lithium Niobate platelet for 5GHz and 13 GHz filters," 2019 IEEE MTT-S International Microwave Symposium (IMS), pp. 512-515, 2019.

[8] R. Lu, Y. Yang, S. Link and S. Gong, "A1 Resonators in 128° Y-cut Lithium Niobate with Electromechanical Coupling of 46.4%," in Journal of Microelectromechanical Systems, vol. 29, no. 3, pp. 313-319.

[9] Y. Osugi, T. Yoshino, K. Suzuki and T. Hirai, "Single crystal FBAR with $LiNbO_3$ and $LiTaO_3$ piezoelectric substance layers," 2007 IEEE/MTT-S International Microwave Symposium, pp. 873-876, 2007.

[10] M. Gorisse *et al.*, "High Frequency $LiNbO_3$ Bulk Wave Resonator," 2019 Joint Conference of the IEEE International Frequency Control Symposium and European Frequency and Time Forum (EFTF/IFCS), pp. 1-2, 2019.

[11] M. Bousquet *et al.*, "Lithium niobate film bulk acoustic wave resonator for sub-6 GHz filters," 2020 IEEE International Ultrasonics Symposium (IUS), pp. 1-4, 2020.

[12] G. Kovacs, M. Anhorn, H. E. Engan, G. Visintini and C. C. W. Ruppel, "Improved material constants for $LiNbO_3$ and $LiTaO_3$," IEEE Symposium on Ultrasonics, vol.1, pp. 435-438, 1990.

[13] M. Bousquet *et al.*, "Single-mode high frequency $LiNbO_3$ Film Bulk Acoustic Resonator," 2019 IEEE International Ultrasonics Symposium (IUS), pp. 84-87, 2019.